Inorganic Chemistry

ARTICLE

pubs.acs.org/IC

Electronic and Molecular Structures of *trans*-Dioxotechnetium(V) Polypyridyl Complexes in the Solid State

Sayandev Chatterjee,[†] Andrew S. Del Negro,[†] Zheming Wang,[‡] Matthew K. Edwards,[†] Frances N. Skomurski,[†] Sean E. Hightower,[†] Jeanette A. Krause,[§] Brendan Twamley,[∥] B. Patrick Sullivan,[⊥] Christian Reber,[#] William R. Heineman,[§] Carl J. Seliskar,[*,§] and Samuel A. Bryan[*,†]

[†]Energy and Environment Directorate, Pacific Northwest National Laboratory, Richland, Washington 99352, United States

[‡]Fundamental and Computational Science Directorate, Pacific Northwest National Laboratory, Richland, Washington 99352, United States

[§]Department of Chemistry, University of Cincinnati, Cincinnati, Ohio 45221, United States

[∥]Department of Chemistry, University of Idaho, Moscow, Idaho 83844, United States

[⊥]Department of Chemistry, University of Wyoming, Laramie, Wyoming 82071, United States

[#]Département de Chimie, Université de Montréal, Montréal QC H3C 3J7, Canada

Supporting Information

ABSTRACT: The structures of novel Tc(V) complexes *trans*-$[TcO_2(py)_4]Cl\cdot 2H_2O$ (**1a**), *trans*-$[TcO_2(pic)_4]Cl\cdot 2H_2O$ (**2a**), and *trans*-$[TcO_2(pic)_4]BPh_4$ (**2b**) were determined by X-ray crystallography, and their spectroscopic characteristics were investigated by emission spectroscopy and atomic scale calculations. The cations adopt a tetragonally distorted octahedral geometry, with a *trans* orientation of the apical oxo groups. *trans*-$[TcO_2(pic)_4]BPh_4$ has an inversion center located on technetium; however, for *trans*-$[TcO_2(py)_4]Cl\cdot 2H_2O$ and *trans*-$[TcO_2(pic)_4]Cl\cdot 2H_2O$, a strong H bond formed by only one of the oxo substituents introduces an asymmetry in the structure, resulting in inequivalent trans Tc−N and Tc═O distances. Upon 415 nm excitation at room temperature, the complexes exhibited broad, structureless luminescences with emission maxima at approximately 710 nm (**1a**) and 750 nm (**2a**, **2b**). Like the Re(V) analogs, the Tc(V) complexes luminesce from a ^3E_g excited state. Upon cooling the samples from 278 to 8 K, distinct vibronic features appear in the spectra of the complexes along with increases in emission intensities. The low temperature emission spectra display the characteristic progressions of the symmetric O═Tc═O and the Tc−L stretching modes. Lowest-energy, triplet excited-state distortions calculated using a time-dependent theoretical approach are in good agreement with the experimental spectra. The discovery of luminescence from the *trans*-dioxotechnetium(V) complexes provides the first opportunity to directly compare fundamental luminescence properties of second- and third-row d^2 metal-oxo congeners.

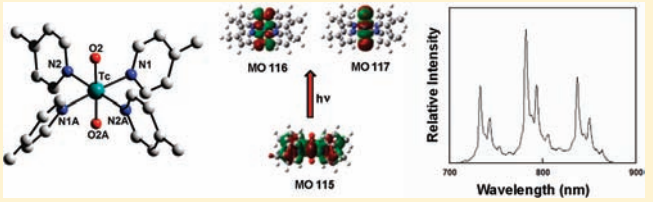

INTRODUCTION

Transition metal complexes with metal−oxygen multiple bonds have been well studied since the benchmark work of Winkler and Gray on the photophysical properties of *trans*-$[ReO_2(L)_4]^+$ (L = pyridine, 4-picoline) in crystalline and solution forms.[1] Similarly, the emission properties of related d^2 dioxoosmium(VI)[2−6] and oxomolybdenum(IV)[7−11] chromophores and electronic structures of d^2 congeners[12] have also been explored. Recently, the work of Reber et al.[13−15] has re-emphasized the importance of *trans*-$[ReO_2(L)_4]^+$ complexes as fundamental models for understanding excited state electronic structure and dynamics in general, with special emphasis on the effect of orbital mixing of the in-plane ligands with the linear ReO_2^+ core, the vibronic coupling between coordinates on the lowest potential emitting surface, and the electronic coupling between the lowest emitting state and higher electronic excited states.[6,13−17]

It is significant to note that unlike the richness in knowledge of dioxorhenium chromophores, there exists a significant dearth in the understanding of the electronic properties of complexes with technetium−oxygen multiple bonds. More specifically, although there have been reports of luminescence of Tc(IV)−halide complexes at low temperatures in a crystalline host matrix,[18−21] or that of a $[Tc(dmpe)_3]_2^+$ complex in the solid state, aqueous solution,[22] or enclosed within a polymer polyelectrolyte,[23,24] extensive studies on the luminescence spectroscopy of technetium dioxo complexes are lacking. Thus, despite well-established studies of the reactivity and spectroscopy of Tc complexes in several oxidation states,[25] not much is known about the electronic spectroscopy of Tc(V) complexes. In a conscious effort to

Received: April 11, 2011
Published: May 24, 2011

bridge this knowledge gap, our group recently reported the first luminescence from a dioxotetrapyridyl Tc(V) complex, with the emission consistent with an excited state having significant metal orbital contribution.[26] While this discovery can pave the way to designing a series of similar dioxo Tc(V) chromophores with long-lived excited states, an in-depth understanding of the systems requires a thorough analysis of the electronic and molecular structures in order to correlate the structural and steric properties with the electronic spectroscopies. However, due to the limited number of reported structures containing technetium−oxygen multiple bonds and the unavailability of spectroscopic data of these crystals, no correlation between electronic and molecular structures of these complexes has been attempted thus far.

In this work, we undertake a thorough and comprehensive study of the electronic structure of two dioxotetrapyridyl Tc(V) complexes through luminescence spectroscopy, which is further substantiated with time-dependent density functional theory (TDDFT/DFT) computational studies. Additionally, in order to gain insight into the molecular structure of the complexes, and in an effort to correlate the molecular structure with the electronic spectra, we are also looking at X-ray intensity data on single crystals of the complexes. Our discovery of room-temperature luminescence from *trans*-dioxotechnetium(V) polypyridyl complexes, and their comparisons with surrogate Re(V) analogs, provides the first opportunity to directly compare fundamental luminescence properties of second- and third-row d^2 metal-oxo congeners. The room- and low-temperature luminescence studies of *trans*-$[TcO_2(L)_4]^+$ (L = pyridine or 4-picoline) reported here, and their correlation with crystal structure analyses, open a new chapter in Tc chemistry, both in a fundamental and in a practical sense.

EXPERIMENTAL SECTION

Radiation safety disclaimer! *Technetium-99 has a half-life of* 2.12×10^5 *years and emits a low-energy (0.292 MeV)* β *particle; common laboratory materials provide adequate shielding. Normal radiation safety procedures must be used at all times to prevent contamination.*

General Considerations. All commercially available chemicals were obtained from Aldrich. $KTcO_4$ was obtained from the Radiochemical Processing Laboratory at Pacific Northwest National Laboratory, from which the complex $[n\text{-}Bu_4N][TcOCl_4]$ was prepared according to the literature,[27] and recrystallized before subsequent use.

UV−visible absorption spectra were recorded using a HP8453 UV−visible spectrophotometer. Emission spectra were recorded using an instrument equipped with a double-emission monochromator and a single-excitation monochromator. Emission spectra were corrected for instrumental response except where noted. The instrumentation and experimental procedures for luminescence spectroscopic measurements at LHeT were described previously.[28,29] Samples in 2 mm × 4 mm quartz cuvettes were mounted on the sample holder of a CRYO Industries RC152 cryostat with liquid helium vaporizing beneath the sample. The sample was excited with a Spectra-Physics Nd:YAG laser-pumped MOPO-730 laser at 415 nm, and the emitted light was collected at 85° to the excitation beam, dispersed through an Acton SpectroPro 300i double-monochromator spectrograph, and detected with a thermoelectrically cooled Princeton Instruments PIMAX intensified CCD camera. The luminescence decay curves were measured with a Hamamatsu R928 photomultiplier tube (PMT) and recorded with a TektronicsTDS754A digital oscilloscope. Microcrystalline solid samples for emission were contained in a silica cell. For lifetime measurements at room temperature, samples were excited using 410−440 nm light from a Continuum Panther optical-parametric oscillator pumped with the third harmonic of a continuum Surelit II Nd:YAG laser. Emission transients were detected using a modified PMT connected to a Tektronix TDS580D oscilloscope and modeled using in-house software on a Microsoft Excel platform. Under these conditions, the emission decay of $[Ru(bpy)_3]Cl_2$ in a 4:1 EtOH/MeOH at 77 K glassy solution was a single exponential corresponding to a lifetime of 5.1 μs, as expected from the literature.[30] Raman spectroscopy measurements were carried out using a Renishaw inVia imaging microscope system. Spectra were obtained using 670 nm laser irradiation on samples in silica cells.

DFT Calculations. Gas-phase, electronic ground-state calculations and geometry optimizations were carried out in Gaussian 03[31] using the B3LYP approximation.[32,33] Time-dependent density functional theory (TDDFT) methods were then used to calculate the 30 lowest-energy singlet and 10 lowest-energy triplet excited states for each compound,[34,35] employing the same B3LYP functional.[26] Calculations utilized the 6-31G* basis set for the ligands and the LANL2DZ relativistic effective core potential (RECP)[36] for the transition metal centers.[37] Symmetry constraints were not imposed on the molecules during geometry optimization. The program AOMix (revision 6.46)[38] was used to analyze molecular orbital occupancy, based on Mulliken population analysis.[39]

Starting models for the compounds of interest were derived from the structural information for $[TcO_2(TBP)_4]CF_3SO_3 \cdot H_2O$(TBP = 4-*tert*-butylpyridine).[40] Models here represent only the cationic centers for the respective complexes; the counterions were not included. Since the structural parameters for complexes **1a**, **2a**, and **2b** do not significantly vary in terms of bond distances observed in the $[TcO_2(TBP)_4]^+$ structure, that structure served as a convenient starting point for the models developed here. Optimized bond lengths for Tc−O and Tc−N are comparable to experimental crystal data for complexes **1a**, **2a**, and **2b** (e.g., $d_{Tc-O(calc)}/d_{Tc-O(exp.ave.)}$[41] = 0.993 for $[TcO_2(py)_4]^+$, 0.997 for $[TcO_2(pic)_4]^+$; $d_{Tc-N(calc)}/d_{Tc-N(exp.ave.)}$[42] = 0.977 for $[TcO_2(py)_4]^+$, 0.978 for $[TcO_2(pic)_4]^+$; see Supporting Information in ref 26 for optimized structural data).

Synthesis. Hydrated forms of yellow microcrystalline samples of *trans*-$[TcO_2(py)_4]Cl \cdot 2H_2O$ (**1a**) and *trans*-$[TcO_2(pic)_4]Cl \cdot 2H_2O$ (**2a**) were obtained by methods similar to literature procedures,[40] by stirring $[n\text{-}Bu_4N][TcOCl_4]$ with the respective pyridine or substituted pyridine ligand at room temperature. The tetraphenylborate salts, *trans*-$[TcO_2(pic)_4]BPh_4$ (**1b**) and *trans*-$[TcO_2(pic)_4]BPh_4$ (**2b**), were obtained by metathesis of the respective chloride salts with $NaBPh_4$ in methanol. The respective chloride and tetraphenylborate salts of *trans*-$[ReO_2(py)_4]^+$ and *trans*-$[ReO_2(pic)_4]^+$ were prepared by literature methods[1,43] in a procedure similar to the synthesis of the Tc analogs.

X-Ray Crystallography. X-ray intensity data for **1a** and **2b** were collected on a Bruker APEX CCD diffractometer (Mo Kα radiation, λ = 0.71073 Å) equipped with a Cryocool NeverIce low-temperature device. Intensity data for **2a** were collected on a Bruker SMART6000 CCD diffractometer (Cu Kα radiation, λ = 1.54178 Å) equipped with an Oxford Cryostream low-temperature device. The data frames were collected using SMART; processed using SAINT; and corrected for decay, Lorentz, and polarization effects as well as absorption and beam corrections based on the multiscan technique in SADABS.[44] The structures were solved by direct methods and refined by full-matrix least-squares on F^2 using SHELXTL.[44] The structures were solved in their respective space groups through an analysis of systematic absences. All non-hydrogen atoms were refined anisotropically. Details of the data collection and refinement are summarized in Table 1. Further details are provided in the Supporting Information. Attempts to grow single crystals of **1b** have yielded amorphous material so far; therefore all measurements for *trans*-$[TcO_2(pic)_4]^+$ were done using the Cl^- salts. $[TcO_2(py)_4]^+$ (**1**) and $[TcO_2(pic)_4]^+$ (**2**) are shown in Scheme 1.

Table 1. Crystal Data and Structure Refinement Data for $[TcO_2(py)_4]Cl\cdot 2H_2O$ (1a), $[TcO_2(pic)_4]Cl\cdot 2H_2O$ (2a), and $[TcO_2(pic)_4]BPh_4$ (2b)

	$[TcO_2(py)_4]Cl\cdot 2H_2O$ (**1a**)	$[TcO_2(pic)_4]Cl\cdot 2H_2O$ (**2a**)	$[TcO_2(pic)_4]BPh_4$ (**2b**)
empirical formula	$C_{20}H_{24}ClN_4O_4Tc$	$C_{24}H_{32}ClN_4O_4Tc$	$C_{48}H_{48}BN_4O_2Tc$
fw	517.88	573.99	821.71
temp (K)	90(2)	90(2)	89(2)
wavelength (Å)	0.71073	1.54178	0.71073
cryst syst	monoclinic	hexagonal	monoclinic
space group	*Cc*	$P6_1$	*C*2/*c*
a (Å)	13.4168(4)	10.2396(1)	8.5028(6)
b (Å)	11.9421(4)	10.2396(1)	19.7612(15)
c (Å)	15.3310(5)	42.6378(8)	24.1525(18)
α (deg)	90	90	90
β (deg)	115.484(1)	90	90.584(1)
γ (deg)	90	120	90
volume ($Å^3$)	2217.41(12)	3871.61(9)	4058.0(5)
Z	4	6	4
density (calcd; Mg/m^3)	1.551	1.477	1.345
abs coeff (mm^{-1})	0.803	5.785	0.399
F(000)	1056	1776	1712
cryst size (mm^3)	0.28 × 0.21 × 0.11	0.10 × 0.07 × 0.04	0.30 × 0.15 × 0.05
cryst color and habit	orange block	orange plate	yellow plate
reflns collected	14048	31951	30087
independent reflns/*R*(int)	5060/0.0205	4677/0.0471	3680/0.0340
max./min transm	0.9169/0.8064	0.8016/0.5954	0.9803/0.8896
data/restraints/params	5060/2/272	4677/1/321	3680/0/257
GOF on F^2	1.041	1.017	1.081
final R indices [$I > 2\sigma(I)$]	0.0218/0.0543	0.0247/0.0595	0.0297/0.0687
R indices (all data) (R1/wR2)	0.0228/0.0550	0.0261/0.0602	0.0349/0.0709

Scheme 1. $[TcO_2(py)_4]^+$ (1) and $[TcO_2(pic)_4]^+$ (2)

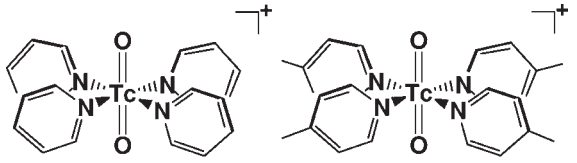

Scheme 2. Synthetic Scheme[a]

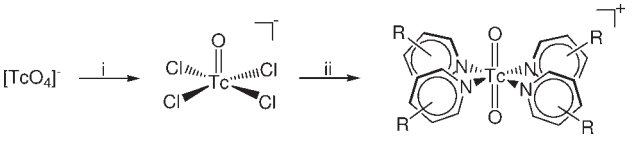

[a] Conditions: (i) Bu_4NCl, HCl; (ii) (a) pyridine; (b) 4-picoline.

SYNTHESIS AND STRUCTURE

The technetium(V) dioxotetraimine complexes were synthesized from the mono-oxo $[TcOCl_4]^-$ precursor, where a combination of $(n\text{-}Bu_4N)[TcOCl_4]$ with the appropriate imine under aerial conditions resulted in complete substitution of the chlorides with four imine ligands, along with the formation of a new Tc(V)−oxo double bond. The synthetic scheme is shown in Scheme 2. The isolated products were crystallized, and the structures of the complexes were determined by X-ray crystallography (Figure 1). Key bond distances and angles are summarized in Table 2.

All cations show a tetragonally distorted octahedral geometry, with a *trans* orientation of the apical oxo groups. The Tc metal center is surrounded by four pyridyl nitrogens in a square planar geometry. The observed Tc−O distances vary from 1.7414(16) to 1.7619(19) Å, comparable to the Re analogs but shorter than observed for *trans*-$K_3[TcO_2(CN)_4]$ (1.7721(12) Å).[45] This shortening is consistent with the electron density of the respective Tc(V) metal centers. The bond distances and angles associated with the ligands are reminiscent of those reported for *trans*-$[TcO_2(TBP)_4]CF_3SO_3\cdot H_2O$ (TBP = 4-*tert*-butylpyridine)[40] and the dioxo-Re analogs.[40,46−57] The plane of the pyridyl rings is rotated away from the O═Tc═O axis with average rotations of 17.53°, 15.45°, and 12.88° for **1a**, **2a**, and **2b**, respectively. Furthermore, two pyridyl rings are rotated in the clockwise direction while the remaining two are rotated counter-clockwise. Specifically, if one focuses on a *trans*-pyridyl ring pair, one notices that they are rotated in opposite directions in **2a**, whereas the same pair of rings are rotated in the same direction in **1a** and **2b**, as well as for *trans*-$[TcO_2(TBP)_4]CF_3SO_3\cdot H_2O$.[40]

It should be noted that the range of Re(V) and Tc(V) structures with the general formula *trans*-$[MO_2(imine)_4]^+$ can be classified as having either two identical M═O bond distances[40,46−51,57] or two

dx.doi.org/10.1021/ic200747v |*Inorg. Chem.* 2011, 50, 5815–5823

Table 2. Bond Lengths [Å] and Angles [deg] for $[TcO_2(py)_4]Cl\cdot 2H_2O$ (1a), $[TcO_2(pic)_4]Cl\cdot 2H_2O$ (2a), and $[TcO_2(pic)_4]BPh_4$ (2b)

	$[TcO_2(py)_4]Cl\cdot 2H_2O$ (**1a**)	$[TcO_2(pic)_4]Cl\cdot 2H_2O$ (**2a**)	$[TcO_2(pic)_4]BPh_4$ (**2b**)[a]
Tc(1)−O(1)	1.7414(16)	1.747(2)	
Tc(1)−O(2)	1.7506(16)	1.762(2)	1.7483(14)
Tc(1)−N(1)	2.142(2)	2.155(2)	2.1487(16)
Tc(1)−N(2)	2.161(2)	2.162(2)	2.1461(17)
Tc(1)−N(3)	2.156(2)	2.157(2)	
Tc(1)−N(4)	2.153(2)	2.164(2)	
O(1)−Tc(1)−O(2)	179.44(10)	178.59(9)	180.00(11)
O(1)−Tc(1)−N(1)	90.95(8)	89.93(9)	
O(1)−Tc(1)−N(2)	89.87(8)	89.70(9)	
O(1)−Tc(1)−N(3)	90.34(8)	90.54(9)	
O(1)−Tc(1)−N(4)	90.31(8)	88.71(9)	
O(2)−Tc(1)−N(1)	89.45(8)	91.37(9)	90.19(6)
O(2)−Tc(1)−N(2)	89.75(7)	89.86(9)	90.16(6)
O(2)−Tc(1)−N(3)	90.03(8)	89.94(9)	89.84(6)
O(2)−Tc(1)−N(4)	89.29(8)	90.01(9)	81.89(6)
N(1)−Tc(1)−N(2)	89.44(8)	86.37(9)	89.32(6)
N(1)−Tc(1)−N(3)	91.47(8)	92.01(9)	
N(1)−Tc(1)−N(4)	178.72(10)	177.35(9)	180.00(7)
N(3)−Tc(1)−N(2)	179.07(9)	178.36(9)	180.00(9)
N(4)−Tc(1)−N(2)	90.31(8)	95.89(9)	90.68(6)
N(3)−Tc(1)−N(4)	88.78(8)	85.74(9)	

[a] Due to the symmetry in **2b**, the corresponding **1a** and **2a** atom names are O1═O2A, N4═N1A, and N3═N2A; refer to the Supporting Information for the complete naming scheme of **2b**.

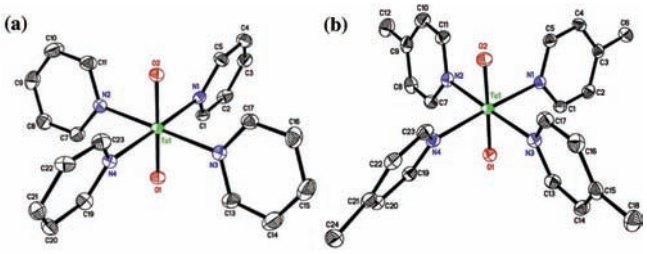

Figure 1. ORTEP diagrams for the cations of (a) $[TcO_2(py)_4]Cl\cdot 2H_2O$ (**1a**) and (b) $[TcO_2(pic)_4]Cl\cdot 2H_2O$ (**2a**) showing the atomic numbering scheme. H atoms and solvent omitted for clarity.

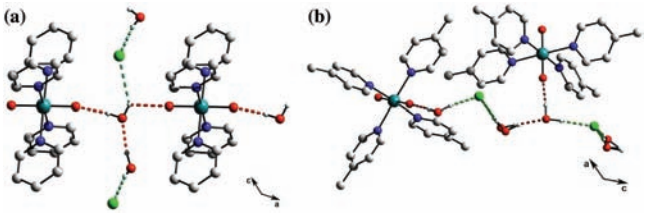

Figure 2. Comparison of the Tc═O···solvent···Cl interactions for $[TcO_2(py)_4]Cl\cdot 2H_2O$ (**1a**; left, **a**) and $[TcO_2(pic)_4]Cl\cdot 2H_2O$ (**2a**; right, **b**). O−H···Cl and O−H···O are shown as green and red dashed lines, respectively. H atoms (with the exception of solvent) are omitted for clarity.

dissimilar M═O distances.[52−56] In most reported cases with dissimilar M═O distances, a solvate molecule is involved in a strong intermolecular interaction with one of the oxo substituents. This is caused by a Tc═O···(solvent) H-bonding interaction and is evidently responsible for the disparity in the distances. The complex *trans*-(phenyl-tris(pyrazolyl)borate-N,N′)-dioxo-bis-(pyridine-N)-rhenium[55] is the only notable exception reported to date, which shows unequal M═O distances even in the absence of a solvent molecule, presumably as a consequence of the steric bulk of the dangling phenyl substituent forcing a nonlinear arrangement with the neighboring oxo substituent. The complex *trans*-$[TcO_2(pic)_4]BPh_4$ (**2b**) crystallizes in a desolvated form while both chloro salts, *trans*-$[TcO_2(pic)_4]Cl\cdot 2H_2O$ (**2a**) and *trans*-$[TcO_2(py)_4]Cl\cdot 2H_2O$ (**1a**), crystallize as dihydrates. Consistent with the above trend, a strong Tc═O···H−O−H···Cl^- interaction (Figure 2) is formed between one of the oxo substituents O(2) and a proton from a solvate water molecule, which introduces an asymmetry in the **1a** and **2a** structures, resulting in inequivalent trans Tc−N and Tc═O distances (Table 2). For **1a**: O(3)···O(2) = 2.759(2) Å, H(3A)···O(2) = 1.91 Å, ∠O(3)−H(3A)···O(2) = 174°, O(4)···Cl(1) = 3.218(2) Å, H(4A)···Cl(1) = 2.38 Å, ∠O(4)−H(4A)···Cl(1) = 170°. For **2a**: O(3)···O(2) = 2.782(3) Å, H(3A)···O(2)= 1.87 Å, ∠O(3)−H(3A)···O(2) = 176°, O(4)···Cl(1) = 3.131(9) Å, H(4A)···Cl(1) = 2.18 Å, ∠O(4)−H(4A)···Cl(1) = 180° and O(4)···Cl(1) = 3.22(3) Å, H(4C)···Cl(1) = 2.31 Å, ∠O(4)−H(4C)···Cl(1) = 166°. A weaker, more bent interaction exists between the solvent water and a neighboring oxo substituent O(1) in the case of **1a** (O3···O(1) = 2.971(2) Å, H(3B)···O(1) = 2.40 Å, ∠O(3)−H(3B)···O(1) = 124°); however, no such interaction exists for **2a**. In addition, the same solvate water molecule O(3) is involved in hydrogen-bonding with the second water molecule (**1a**: O(4)···O(3) = 2.735(2) Å, H(4B)···O(3)

dx.doi.org/10.1021/ic200747v |*Inorg. Chem.* 2011, 50, 5815–5823

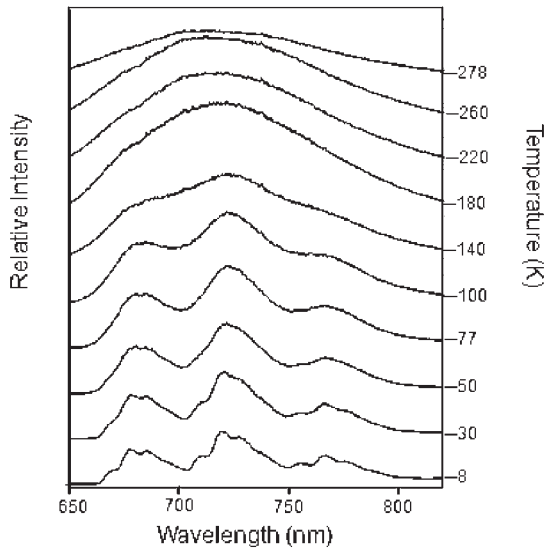

Figure 3. Temperature dependent luminescence behavior of $[TcO_2(py)_4]Cl\cdot 2H_2O$ (**1a**).

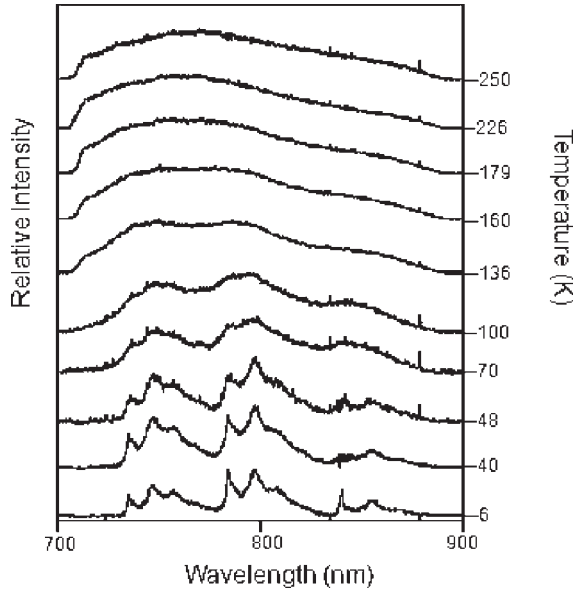

Figure 4. Temperature dependent luminescence behavior of $[TcO_2(pic)_4]Cl\cdot 2H_2O$ (**2a**).

= 1.89 Å; ∠O(4)−H(4B)···O(3) = 171°. **2a**: O(4)···O(3) = 2.902(8) Å, H(4B)···O(3) = 1.96 Å; ∠O(4)−H(4B)···O(3) = 180° and O(4)···O(3) = 2.67(3) Å, H(4D)···O(3) = 1.76 Å; ∠O(4)−H(4D)···O(3) = 157°).

In the absence of hard, electron-deficient centers in the proximity of the oxo substituents, the Tc═O distances in **2b** are identical. Furthermore, one of the picoline rings of the **2b** cation is involved in a π-stacking interaction with a phenyl group of the BPh_4^- counterion. It is to be noted that structures with identical M═O distances are symmetric with a D_{2h} point group, where the trans M−N distances and trans angles are identical. On the other hand, structures with dissimilar M═O bond distances are observed to have no intrinsic symmetry, resulting in a C_1 point group. Furthermore, for structures with identical M═O distances, the metal center lies in the plane of the imine nitrogens, while those with dissimilar metal−oxo distances have the metal displaced from the imine nitrogen plane, resulting in a pyramidal geometry.

Table 3. Parameters Used to Calculate Luminescence Spectra[a]

parameter	$TcO_2(pic)_4^+$	$ReO_2(pic)_4^+$	$TcO_2(py)_4^+$	$ReO_2(py)_4^+$
E_{00} [cm^{-1}]	13650	16180	14900	16400
ν(M═O) [cm^{-1}]	852	900	854	905
$\Delta_{M=O}$ [dim.less]	1.90	1.83	2.00	1.75
ν(M−L) [cm^{-1}]	188	210	167	193
Δ_{M-L} [dim.less]	1.01	1.01	1.9	1.24
ν_3 [cm^{-1}]	98	n/a	n/a	n/a
Δ_3 [dim.less]	0.82	n/a	n/a	n/a
Γ [cm^{-1}]	23	45	45	50

[a] Harmonic potential energy surfaces with identical force constants in the ground and emitting states were used. Parameters are defined in eq 1 and discussed in the text.

SPECTROSCOPY AND CALCULATIONS

In order to explore the electronic structure of the *trans*-$[TcO_2(L)_4]^+$ complexes and their measured emission spectroscopy further, Franck−Condon analysis of the spectroscopic data and density functional theory calculations were performed.

Emission Spectroscopy and Franck−Condon Analysis. The complexes **1a**, **2a**, and **2b** crystallized as yellow or orange-yellow blocks. Upon excitation (λ_{exc} = 415 nm) at room temperature, the crystals exhibited broad, structureless luminescence features with emission maxima at ∼710 nm (**1**) and ∼750 nm (**2a**, **2b**), respectively. These emissions are significantly red-shifted compared to their Re analogs.

Upon cooling the crystals from 278 to 8 K, distinct vibronic features appear in the spectra of **1a**, **2a**, and **2b** along with increase in emission intensities. Figures 3, 4, and S5 (Supporting Information) show temperature-dependent luminescence spectra for **1a**, **2a**, and **2b**. At least two vibronic progressions are observed in the low-temperature spectra: one progression is clearly visible at temperatures below 100 K, and a second lower-frequency progression appears below 30 K (*vide infra*), superimposed on the first. By analogy to similar Re(V) complexes, the low-temperature emission spectra of **1a** and **2a** appear to display progressions characteristic of the symmetric O═Tc═O and the Tc−L stretching modes (Figures 3 and 4). The room temperature emission spectra of Tc(V)−dioxo complexes and those for their Re(V) surrogates are shown in Figure S8 (Supporting Information). Thus, the observed O═Tc═O vibronic progression (∼850 cm^{-1}) is consistent with the Raman active O═Tc═O symmetric stretches of 856 and 852 cm^{-1} for **1a** and **2a**, respectively, and is ca. 50 cm^{-1} lower compared to the corresponding Re complexes (see Table 3). It should be noted that the low-temperature spectrum of **2b** is significantly more resolved than that of **2a**. In fact, the low-temperature (6 K) spectrum for **2b** shown in Figure 5 is the most resolved spectrum of *trans*-dioxotetraiminotechnetium(V) measured to date. Presumably, this is consistent with the higher symmetry of the **2b** complex as compared to **1a** and **2a**. Furthermore, it clearly shows the lower energy (∼180−200 cm^{-1}) progression that is consistent with a Tc−L mode found for the corresponding *trans*-dioxorhenium

dx.doi.org/10.1021/ic200747v |*Inorg. Chem.* 2011, 50, 5815–5823

analogues. The well-resolved vibronic structure of the luminescence spectra is analyzed below.

Excited-state lifetimes were measured for the complexes at room and low temperatures. For standardization, the lifetime of *trans*-$[ReO_2(py)_4]^+$ was determined, and the experimental value (near the liquid helium temperature) of 68 μs acquired here is close to the lifetime reported.[1] For all cases at 8 K, the excited-state lifetimes were fit to a single exponential decay. At 8 K, the lifetimes for **1a** and **2b** were 78 and 15 μs, respectively, and are to be compared with the 71 and 48 μs lifetimes measured for the corresponding Re(V) complexes.

It was also observed that the temperature-dependent emission spectra of 2a showed a dependence on the delay time after the pulsed laser excitation. Thus, upon excitation at 415 nm, an intense band around 690 nm was observed after a time delay of more than 50 μs with a wide gatewidth (5 ms) at 6 K. The intensity of the band gradually decreases as the temperature is raised. The same band was absent within the first 50 μs after laser excitation. These observations are consistent with the presence of multiple excited states in the sample with different fluorescence lifetimes. This feature was reproduced in multiple batches of samples. While the exact origin of this band is uncertain at the moment, it should be noted that it was not generated from the $[TcOCl_4]^-$ starting material, as this species is nonemissive upon 415 nm excitation. The exact origin of this band is presently under investigation.

The well-resolved vibronic structure in the luminescence spectra shown in Figures 3 and 4 can be used to determine quantitative structural changes in the emitting state. Calculated luminescence spectra based on harmonic potential energy surfaces with identical vibrational frequencies for the ground and emitting states are compared to the experimental spectra; parameters are adjusted until a satisfactory agreement is obtained. Spectra were calculated using the time-dependent theoretical approach.[58−60] The luminescence intensity is given by

$$I(\omega) = C\omega^3 \int_{-\infty}^{\infty} e^{i\omega t} \exp\left(\sum_i -\left[\frac{\Delta_i^2}{2}(1 - e^{-i\omega_i t}) - \frac{i\omega_i t}{2}\right] - iE_{00}t - \Gamma^2 t^2\right) dt \quad (1)$$

where ω denotes the wavenumber range, E_{00} is the energy of the highest-energy transition used in the calculation, i is the number of normal coordinates, Δ_i is the offset between ground- and emitting-state potential energy minima along a normal coordinate i in dimensionless units, and Γ is a Gaussian damping factor that determines the width of each vibronic line. The calculated luminescence spectra are in good agreement with the experimental spectra, as shown in Figure 6. The parameter values obtained for all calculated luminescence spectra are summarized in Table 3. A baseline corresponding to an unresolved spectrum, possibly arising from imperfect crystal sites, is added to some calculated spectra in order to improve the agreement in the regions of low intensity between vibronic peaks. This addition does not influence the parameter values in Table 3.

The electronic origins of the luminescence spectra of *trans*-dioxo complexes are often weak and have been identified in a few cases from well-resolved absorption and luminescence spectra.[1] The more intense peaks corresponding to the highest-energy transitions in the calculated spectra most likely have vibronic origins, involving one quantum of ungerade parity modes leading

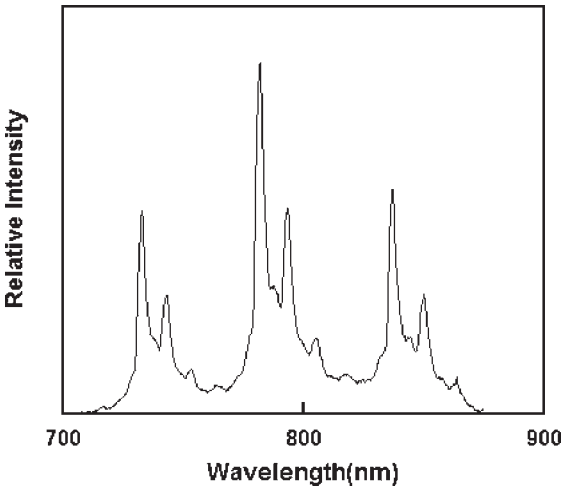

Figure 5. Luminescence spectrum of $[TcO_2(pic)_4]BPh_4$ (**2b**) at 6 K.

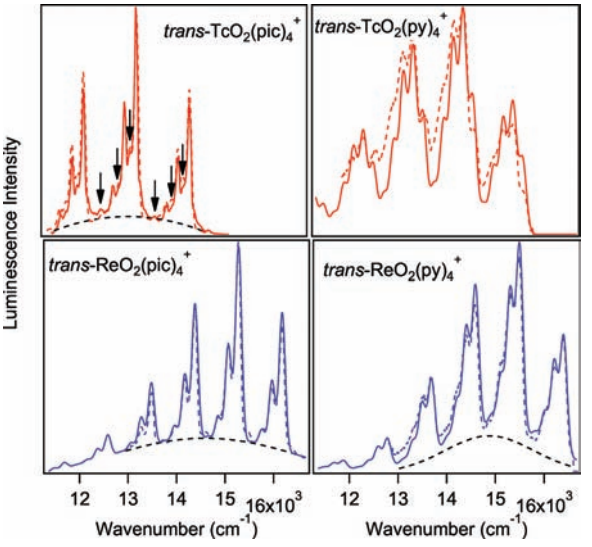

Figure 6. Comparison of experimental and calculated luminescence spectra. All spectra are represented in the same wavenumber range. Calculated spectra are shown as solid lines and experimental spectra as dotted lines. The black dotted lines show the baseline added to the calculated spectra. For the picolyl complexes, the experimental data for BPh_4^- were considered. For the pyridyl complexes, the data for Cl^- salts were compared with calculated spectra.

to a more highly allowed transition. Complexes **1** and **2** have E_{00} values lower by 1500 cm^{-1} for **1** and 2530 cm^{-1} for **2** than their rhenium analogs.

Offsets Δ_i along the normal coordinates with prominent vibronic progressions have been determined for many Re(V) complexes[1,6−11,13,15−17] but not for Tc(V) complexes. The calculated spectra in Figure 6 show that offsets Δ_i along the Re−oxo normal coordinate are similar to the literature values of 1.95−2.18.[1,6−11,13,15−17] The Tc complexes have offsets $\Delta_{M=O}$ higher by approximately 5% than their Re analogs, indicating a slightly stronger π^* character of the $d_{xz,yz}$ LUMO orbitals in the Tc complexes. These results are in qualitative agreement with the higher O(p) character obtained from the DFT calculations in this study. This first comparison of $\Delta_{M=O}$ values for corresponding *trans*-dioxo complexes of second- and third-row metals illustrates

dx.doi.org/10.1021/ic200747v |*Inorg. Chem.* 2011, 50, 5815–5823

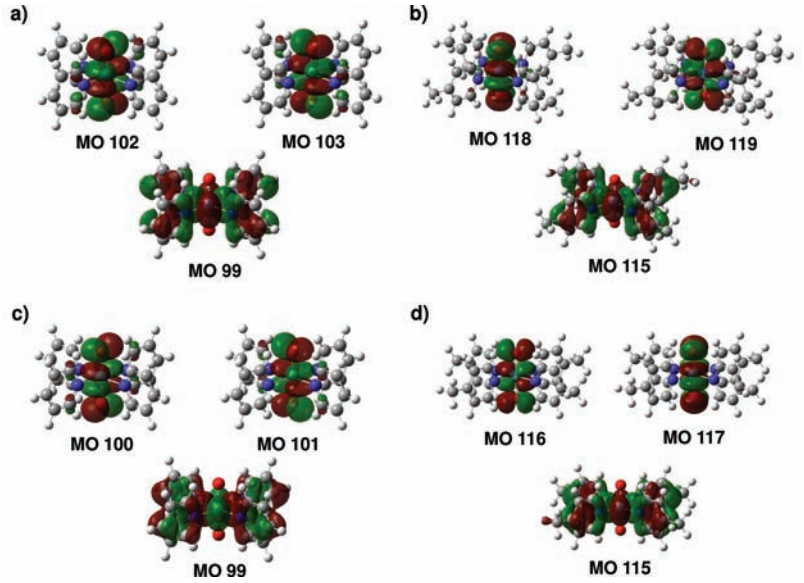

Figure 7. Electron-density maps of selected MOs projected onto optimized structures of (a) *trans*-$[ReO_2(py)_4]^+$, (b) *trans*-$[ReO_2(pic)_4]^+$, (c) *trans*-$[TcO_2(py)_4]^+$, and (d) *trans*-$[TcO_2(pic)_4]^+$. Central, light-blue spheres are Tc(V) and Re(V). Red spheres are O. Dark blue spheres are N. Dark gray spheres are C, and light gray spheres are H.

that the established overall trend of increasing ligand field splittings leading to larger offsets Δ_i for heavier metal centers is not universal.

The offsets along the metal-ancillary coordinates are similar for the (pic) complexes **2** and the Re analogs. A larger value is obtained for the Tc complex **1** than for its Re analog. The spectrum of complex **2** has the most highly resolved vibronic structure, leading to a vibronic line width Γ of 23 cm^{-1}, which is lower than for the other complexes by approximately a factor of 2. This spectrum of *trans*-$[TcO_2(pic)_4]^+$ in the top, left-hand panel of Figure 6 shows a regular sequence of peaks denoted by vertical arrows with energy differences not corresponding to either the Tc−oxo or Tc−pic modes. They can be reproduced by including a third normal coordinate with nonzero offset in the calculations, as given in Table 3. As an alternative, they could be due to a replica of the vibronic structure built on a less efficient vibronic origin at higher frequency than the most intense progressions. Multiple vibronic origins have been identified in the luminescence spectra of several *trans*-dioxo rhenium(V) complexes. The values of $\Delta_{M=O}$ and Δ_{M-L} do not depend on the choice of assignment for the transitions denoted by the vertical arrows. Similar detailed features are not apparent in the less resolved luminescence spectra of the other complexes.

Density Functional Theory/Time-Dependent Density Functional Theory Calculations. On the basis of the analysis of 30 singlet and 10 triplet excited-state calculations for each complex, computational results indicate the dioxotechnetium emission to be about 0.41 eV lower in energy than the dioxorhenium counterparts for both the tetrapyridyl and tetrapicolyl complexes.[61] Excitation energies and oscillator strengths of the lowest energy, triplet excited-state transitions are shown in Table S1 (Supporting Information). While the magnitude of this value is higher than the numeric value of 0.21 eV obtained experimentally,[26] it correctly predicts the red-shift of the emissions from **1a**, **2a**, and **2b** compared to the *trans*-$[ReO_2(L)_4]^+$ analogs.[26,37] Similar to the Re analog, the Tc complex luminesces from an ^3E_g excited state. For *trans*-$[ReO_2(py)_4]^+$, the calculations predict that the major contributing excitation is from the pair MO 99 (HOMO) to the degenerate pair MO 102 (LUMO+1) and MO 103 (LUMO+1′) (see Figure 7a). MO 99 has 71% Re(d) (mostly d_{xy}) and 29% p_y character, while MOs 102 and 103 have 55% Re(d) and 39% O(p) character (see Table S1, Supporting Information, for complete molecular orbital characterization results). For *trans*-$[ReO_2(pic)_4]^+$, a similar transition is observed from the pair MO 115 (HOMO) to the pair MO 118 (LUMO+1) and MO 119 (LUMO+1′) (see Figure 7b). While the major contributions to the orbital character of the HOMO are similar to *trans*-$[ReO_2(py)_4]^+$, electron density is more evenly distributed between the Re(d_{xz}) and Re(d_{xy}) LUMO orbitals than in the previous case (see Table S2, Supporting Information).

A similar trend exists for the excited-state transition of *trans*-$[TcO_2(L)_4]^+$ (where L = py or pic). For *trans*-$[TcO_2(py)_4]^+$, the major contributions are excitations from the pair MO 99 (HOMO) to MO 100 (LUMO) and MO 101 (LUMO′) (see Figure 7c). Here, MO 99 has 73% Tc(d_{yz}) and 27% O(p) character, and MOs 100 and 101 have 56 Tc(d) and 41% O(p) character, which is similar to electron density distributions for *trans*-$[ReO_2(py)_4]^+$ (see Table S2, Supporting Information). For *trans*-$[TcO_2(pic)_4]^+$, major contributions are from the pair MO 115 (HOMO) to MO 116 (LUMO) and MO 117 (LUMO′) (see Figure 7d). Here too, the characters for MO 115, 116, and 117 are similar to the *trans*-$[ReO_2(pic)_4]^+$ case, where major HOMO contributions are 70% Tc(d_{yz}) and 30% pic, and major LUMO contributions are approximately 28% for both Tc (or Re) d_{xz} and d_{yz} orbitals and 41% from the axial oxygens O(p) (see Table S2, Supporting Information). The cumulative observations are suggestive that the choice of the metal center has a significant effect on determining the nature of the transition (e.g., HOMO → LUMO+1 for Re versus HOMO → LUMO for Tc); on the other hand, the imine substituents have a significantly weaker influence on the transitions.

For *trans*-$[TcO_2(py)_4]^+$, a small but significant difference from *trans*-$[ReO_2(py)_4]^+$ is the contribution of the excitation

dx.doi.org/10.1021/ic200747v |*Inorg. Chem.* 2011, 50, 5815–5823

from MO 86 to MOs 100 and 101. Since MO 86 has an 85% py and 15% Tc(d_{yz}) character (see Figure S10a, Supporting Information), this imparts both ligand-to-metal charge-transfer (LMCT) and ligand-to-ligand charge-transfer (LLCT) character to the transition. A similar contribution also exists for *trans*-$[TcO_2(pic)_4]^+$, from MO 104 to MOs 116 and 117 (see Figure S10b, Supporting Information). Here, MO 104 is 82% pic in character and 18% Tc(d_{yz}). This contribution is not observed for the lowest-energy excited transitions for *trans*-$[ReO_2(py)_4]^+$.[26] This calculated energetic order and character of the HOMO and LUMO orbitals is observed for a variety of *trans*-dioxo complexes with different functionals.[62]

CONCLUSIONS

This work gives a detailed look at the solid-state molecular and electronic structures of two novel Tc(V) complexes, *trans*-$[TcO_2(py)_4]^+$ and *trans*-$[TcO_2(pic)_4]^+$. Both complexes show an intense structureless emission band at room temperature upon excitation by 415 nm laser light. At lower temperatures, the structureless band resolves into vibronic structures consistent with Tc═O and imine stretching modes. On the basis of comparison of the spectra of **2a** and **2b** at 6 K, the resolution of the band depends upon the symmetry of the molecule, as expected; the higher the symmetry, the greater the resolution. The emission maxima for the complexes are red-shifted from the Re(V) analogs, as predicted by TDDFT/DFT calculations. The transitions are very similar to the Re(V) analogs in having a significant MLCT character; however, the significant pyridine character of the HOMOs for the Tc(V) complexes impart a small but significant LLCT contribution to the transition.

This work presents the first comprehensive look at the electronic structures of Tc(V) dioxo tetrapyridyl complexes. The metal-centered luminescence properties of these complexes arising from the radionuclide technetium-99 open up the possibility of using these complexes as imaging agents for bioanalytical applications.

ASSOCIATED CONTENT

Supporting Information. Figures S1−S10 and Tables S1 and S2, crystallographic data in CIF format for all compounds, and a complete ref 31 are provided. This material is available free of charge via the Internet at http://pubs.acs.org.

AUTHOR INFORMATION

Corresponding Author

*E-mail: seliskcj@ucmail.uc.edu and sam.bryan@pnnl.gov.

ACKNOWLEDGMENT

Support from the Office of Environmental Management Sciences Program of the U.S. Department of Energy (Grant DE-FG0799ER62331) is greatly acknowledged. Part of this research was performed at EMSL, a national scientific user facility at PNNL managed by the Department of Energy's Office of Biological and Environmental Research. Pacific Northwest National Laboratory is operated for the U.S. Department of Energy by Battelle under Contract DE-AC06-76RLO 1830. Support from the Hans and Marlies Zimmer International Scholar Fund (University of Cincinnati) for the extended visit of C.R. to the Department of Chemistry is gratefully acknowledged. Funding for the SMART6000 diffractometer was through NSF-MRI (grant CHE-0215950). The SMART APEX Diffraction Facility (University of Idaho) was funded by NSF-EPSCoR and M.J. Murdock Charitable Trust, Vancouver, Washington.

REFERENCES

(1) Winkler, J. R.; Gray, H. B. *Inorg. Chem.* **1985**, *24*, 346.
(2) Cheng, J. Y. K.; Cheung, K. K.; Che, C. M.; Lau, T. C. *Chem. Commun.* **1997**, 1443.
(3) Grey, J. K.; Butler, I. S.; Reber, C. *Inorg. Chem.* **2004**, *43*, 5103.
(4) Schindler, S.; Castner, E. W.; Creutz, C.; Sutin, N. *Inorg. Chem.* **1993**, *32*, 4200.
(5) Yam, V. W. W.; Che, C. M. *Coord. Chem. Rev.* **1990**, *97*, 93.
(6) Savoie, C.; Reber, C. *J. Am. Chem. Soc.* **2000**, *122*, 844.
(7) Isovitsch, R. A.; Beadle, A. S.; Fronczek, F. R.; Maverick, A. W. *Inorg. Chem.* **1998**, *37*, 4258.
(8) Isovitsch, R. A.; May, J. G.; Fronczek, F. R.; Maverick, A. W. *Polyhedron* **2000**, *19*, 1437.
(9) Mohammed, A. K.; Maverick, A. W. *Inorg. Chem.* **1992**, *31*, 4441.
(10) Da Re, R. E.; Hopkins, M. D. *Inorg. Chem.* **2002**, *41*, 6973.
(11) Lanthier, E.; Bendix, J.; Reber, C. *Dalton Trans.* **2010**, *39*, 3695.
(12) *Electronic Structure of Metal-Oxo Complexes*; Miskowski, V. M., Gray, H. B., Hopkins, M. D., Eds.; JAI Press Inc.: Greenwich, CT, 1996; Vol. 1.
(13) Savoie, C.; Reber, C. *Coordin Chem Rev* **1998**, *171*, 387.
(14) Savoie, C.; Reber, C. *Abstr. Pap.—Am. Chem. Soc.* **1995**, *209*, 293.
(15) Savoie, C.; Reber, C.; Belanger, S.; Beauchamp, A. L. *Inorg. Chem.* **1995**, *34*, 3851.
(16) Grey, J. K.; Butler, I. S.; Reber, C. *J. Am. Chem. Soc.* **2002**, *124*, 11699.
(17) Grey, J. K.; Butler, I. S.; Reber, C. *Can. J. Chem.* **2004**, *82*, 1083.
(18) Flint, C. D.; Lang, P. *J. Lumin.* **1981**, *24*−*5*, 301.
(19) Flint, C. D.; Lang, P. F. *J. Chem. Soc., Faraday Trans. II* **1986**, *82*, 465.
(20) Flint, C. D.; Lang, P. F. *J. Chem. Soc., Dalton Trans.* **1986**, 921.
(21) Wendt, A.; Preetz, W. *Z. Naturforsch., A: Phys. Sci.* **1992**, *47*, 882.
(22) Del Negro, A. S.; Seliskar, C. J.; Heineman, W. R.; Hightower, S. E.; Bryan, S. A.; Sullivan, B. P. *J. Am. Chem. Soc.* **2006**, *128*, 16494.
(23) Chatterjee, S.; Del Negro, A. S.; Edwards, M. K.; Bryan, S. A.; Kaval, N.; Pantelic, N.; Morris, L. K.; Heineman, W. R.; Seliskar, C. J. *Anal. Chem.* **2011**, *83*, 1766–1772.
(24) Chatterjee, S.; Del Negro, A. S.; Hightower, S. E.; Wang, Z.; Bryan, S. A.; Sullivan, B. P.; Heineman, W. R.; Seliskar, C. J. Manuscript in preparation 2011.
(25) Schwochau, K. *Technetium: Chemistry and Radiopharmaceutical Applications*; Wiley-VCH: New York, 2000.
(26) Del Negro, A. S.; Wang, Z. M.; Seliskar, W. R.; Heineman, W. R.; Sullivan, B. P.; Hightower, S. E.; Hubler, T. L.; Bryan, S. A. *J. Am. Chem. Soc.* **2005**, *127*, 14978.
(27) Cotton, F. A.; Davison, A.; Day, V. W.; Gage, L. D.; Trop, H. S. *Inorg. Chem.* **1979**, *18*, 3024.
(28) Wang, Z. M.; Zachara, J. M.; Yantasee, W.; Gassman, P. L.; Liu, C. X.; Joly, A. G. *Environ. Sci. Technol.* **2004**, *38*, 5591.
(29) Wang, Z. M.; Zachara, J. M.; McKinley, J. P.; Smith, S. C. *Environ. Sci. Technol.* **2005**, *39*, 2651.
(30) Crosby, G. A.; Perkins, W. G.; Klassen, D. M. *J. Chem. Phys.* **1965**, *43*, 1498.
(31) Frisch, M. J.; Trucks, G. W.; Schlegel, H. B.; Scuseria, G. E.; Robb, M. A.; Cheeseman, J. R.; Montgomery, J. A., Jr.; Vreven, T.; Kudin, K. N.; Burant, J. C.; Millam, J. M.; Iyengar, S. S.; Tomasi, J.; Barone, V.; Mennucci, B.; Cossi, M.; Scalmani, G.; Rega, N.; Petersson, G. A.; Nakatsuji, H.; Hada, M.; Ehara, M.; Toyota, K.; Fukuda, R.; Hasegawa, J.; Ishida, M.; Nakajima, T.; Honda, Y.; Kitao, O.; Nakai, H.; Klene, M.; Li, X.; Knox, J. E.; Hratchian, H. P.; Cross, J. B.; Bakken, V.; Adamo, C.; Jaramillo, J.; Gomperts, R.; Stratmann, R. E.; Yazyev, O.; Austin, A. J.; Cammi, R.; Pomelli, C.; Ochterski, J. W.; Ayala, P. Y.; Morokuma, K.; Voth, G. A.; Salvador, P.; Dannenberg, J. J.;

Zakrzewski, V. G.; Dapprich, S.; Daniels, A. D.; Strain, M. C.; Farkas, O.; Malick, D. K.; Rabuck, A. D.; Raghavachari, K.; Foresman, J. B.; Ortiz, J. V.; Cui, Q.; Baboul, A. G.; Clifford, S.; Cioslowski, J.; Stefanov, B. B.; Liu, G.; Liashenko, A.; Piskorz, P.; Komaromi, I.; Martin, R. L.; Fox, D. J.; Keith, T.; Al-Laham, M. A.; Peng, C. Y.; Nanayakkara, A.; Challacombe, M.; Gill, P. M. W.; Johnson, B.; Chen, W.; Wong, M. W.; Gonzalez, C.; Pople, J. A. *Gaussian 03*; Gaussian, Inc.: Wallingford CT, 2004.

(32) Lee, C. T.; Yang, W. T.; Parr, R. G. *Phys. Rev. B* **1988**, *37*, 785.

(33) Becke, A. D. *J. Chem. Phys.* **1993**, *98*, 5648.

(34) Runge, E.; Gross, E. K. U. *Phys. Rev. Lett.* **1984**, *52*, 997.

(35) Gross, E. K. U.; Kohn, W. *Phys. Rev. Lett.* **1985**, *55*, 2850.

(36) Hay, P. J.; Wadt, W. R. *J. Chem. Phys.* **1985**, *82*, 299.

(37) Frisch, M. J. et al. *Gaussian 03*, Revision C.02; Gaussian, Inc.: Wallingford, CT, 2004.

(38) Gorelsky, S. I.; Lever, A. B. P. *J. Organomet. Chem.* **2001**, *635*, 187.

(39) Mulliken, R. S. *J. Chem. Phys.* **1955**, *23*, 1833.

(40) Kastner, M. E.; Fackler, P. H.; Clarke, M. J.; Deutsch, E. *Inorg. Chem.* **1984**, *23*, 4683.

(41) $d_{Tc-O(exp.ave.)}$ for $[TcO_2(py)_4]^+$ is the average of two inequivalent Tc−O distances observed in **1a**, and for $[TcO_2(pic)_4]^+$, it is the average of three inequivalent Tc−O distances observed in **2a** and **2b**.

(42) $d_{Tc-N(exp.ave.)}$ for $[TcO_2(py)_4]^+$ is the average of four inequivalent Tc−N distances observed in **1a**, and for $[TcO_2(pic)_4]^+$ it is the average of six inequivalent Tc−N distances observed in **2a** and **2b**.

(43) Beard, J. H.; Calhoun, C.; Casey, J.; Murmann, R. K. *J. Am. Chem. Soc.* **1968**, *90*, 3389.

(44) *SMART*, v5.630 & 5.634; *SAINT*, v7.23A & 7.66A; Bruker Analytical X-ray Instruments, Inc., Madison, WI. For the application of semi-empirical absorption and beam corrections: Sheldrick, G. M. *SADABS*, v2.01 & 2008/1; University of Göttingen: Göttingen, Germany. For structure solution, ORTEP figures and tables, neutral-atom scattering factors as stored in this package: Sheldrick, G. M. *SHELXTL*, v6.14; University of Göttingen: Göttingen, Germany; Bruker Analytical X-ray Instruments, Inc.: Madison, WI. For extended packing figures: Brandenburg, K. *DIAMOND*, v3.2e; Crystal Impact GbR: Bonn, Germany.

(45) Chatterjee, S.; Del Negro, A. S.; Edwards, M. K.; Twamley, B.; Krause, J. A.; Bryan, S. A. *Acta Crystallogr., Sect. E* **2010**, *66*, I61.

(46) Reddy, K. R.; Domingos, A.; Paulo, A.; Santos, I. *Inorg. Chem.* **1999**, *38*, 4278.

(47) Johnson, J. W.; Brody, J. F.; Ansell, G. B.; Zentz, S. *Inorg. Chem.* **1984**, *23*, 2415.

(48) Kochel, A. *Acta Crystallogr., Sect. E* **2006**, *62*, M1740.

(49) Luck, R. L.; O'Neill, R. S. *Polyhedron* **2001**, *20*, 773.

(50) Brewer, J. C.; Thorp, H. H.; Slagle, K. M.; Brudvig, G. W.; Gray, H. B. *J. Am. Chem. Soc.* **1991**, *113*, 3171.

(51) Fackler, P. H.; Lindsay, M. J.; Clarke, M. J.; Kastner, M. E. *Inorg. Chim. Acta* **1985**, *109*, 39.

(52) Gerber, T. I. A.; Hosten, E.; Tshentu, Z. R.; Mayer, P.; Perez-Carreno, E.; Garcia-Granda, S.; Du Preez, J. G. H. *J. Coord. Chem.* **2003**, *56*, 1063.

(53) Calvo, C.; Krishnamachari, N.; Lock, C. J. L. *J. Cryst. Mol. Struct.* **1971**, 161.

(54) Lock, C. J. L.; Turner, G. *Acta Crystallogr., Sect. B* **1978**, *34*, 923.

(55) Garcia, R.; Xing, Y. H.; Domingos, A.; Paulo, A.; Santos, I. *Inorg. Chim. Acta* **2003**, *343*, 27.

(56) Paulo, A.; Reddy, K. R.; Domingos, A.; Santos, I. *Inorg. Chem.* **1998**, *37*, 6807.

(57) Siczek, M.; Krawczyk, M. S.; Lis, T. *Acta Crystallogr., Sect. E* **2009**, *65*, M1057.

(58) Heller, E. J. *Acc. Chem. Res.* **1981**, *14*, 368.

(59) Zink, J. I. *Coord. Chem Rev* **2001**, *211*, 69.

(60) Zink, J. I.; Shin, K. S. K. *Adv. Photochem.* **1991**, *16*.

(61) Sullivan, B. P. d. Unpublished results, 2008. Electronic ground state and geometry optimization were carried out using the B3LYP approximation, followed by TDDFT calculation of the lowest excited states employing the same functional. Calculations utilized the 6-31G* basis set for the ligands and the LANL2 relativistic effective core potential (RECP) for the transition metal.

(62) Hummel, P.; Winkler, J. R.; Gray, H. B. *Dalton Trans.* **2006**, 168.